UGC Major Research Project Final Report
(F. No. 39-548/2010 (SR))

For the duration (01.02.2011 to 31.01.2014)

On the project titled

"Shape and chemical feature based 3D- pharmacophore model generation, virtual screening and MESP studies to identify potential leads for antifungal azoles"

Submitted to

University Grants Commission
Bahadurshah Zafar Marg
New Delhi-110 002

Submitted by

Dr. Sanjeev Kumar Singh
Associate Professor
Department of Bioinformatics, Alagappa University
Karaikudi- 630 004, Tamil Nadu

UNIVERSITY GRANTS COMMISSION
BAHADUR SHAH ZAFAR MARG

NEW DELHI – 110 002

PROFORMA FOR SUBMISSION OF INFORMATION AT THE TIME OF SENDING THE FINAL REPORT OF THE WORK DONE ON THE PROJECT

1. NAME AND ADDRESS OF THE PRINCIPAL INVESTIGATOR:

Dr. Sanjeev Kumar Singh

Department of Bioinformatics

Alagappa University

Karaikudi-630 004, Tamil Nadu

2. NAME AND ADDRESS OF THE INSTITUTION:

Alagappa University

Karaikudi-630 003, Tamil Nadu

3. UGC APPROVAL NO. AND DATE : **F. No. 39-548/2010 (SR) dated 10.01.2011**

4. DATE OF IMPLEMENTATION : **01.03.2011**

5. TENURE OF THE PROJECT : **Three years (01.02.2011 to 31.01.2014)**

6. TOTAL GRANT ALLOCATED : **Rs. 7,82,348/-**

7. TOTAL GRANT RECEIVED : **Rs. 7,82,348/-**

8. FINAL EXPENDITURE : **Rs. 7,79,957/-**

9. TITLE OF THE PROJECT : **Shape and chemical feature based 3D- pharmacophore model generation, virtual screening and MESP studies to identify potential leads for antifungal azoles**

10. OBJECTIVES OF THE PROJECT:

- **Selection of clinically used structurally diverse set of antifungal azoles.**
- **3D-pharmacophore model generation based on shape and chemical features on selected ligands, co-crystallized with 14 α-demethylase enzyme.**
- **Extraction of Pharmacophore for understanding of key functional groups and atoms play important role in active Pharmacophore.**
- **Searching of pharmacophoric features in Small molecule database like ASINEX and CSD to get hits.**
- **Generation of combinatorial libraries based on important functional group and hits.**
- **Primary filtering of molecules based on Lipinski's rule-of-five and restricting the number of rotatable bonds ≤7 to reduce the dataset.**
- **Comparison of co-crystallized wild and mutant type of 14 α-demethylase enzyme to be used as protein for Induced Fit Docking (IFD).**
- **Analysis of active site or binding site of targeted wild and mutant type of 14 α-demethylase enzymes.**
- **Perform Induced Fit Docking on known and unknown compounds for both wild type and mutant protein.**
- **Analysis and refinement of new leads for mutant type of 14 α-demethylase enzyme based on biological and physio-chemical properties of existing compounds.**
- **Further screening potential inhibitors for antifungal based on (i) fitness scores (ii) binding scores (iii) mode of binding and (iv) interactions with the key amino acid residues.**
- **MESP calculation on selected compounds to understand the complete charge environment.**
- **Predication of ADME/T properties of screened compounds.**

11. WHETHER OBJECTIVES WERE ACHIEVED (GIVE DETAILS):

The objectives of this study are achieved with satisfactory results. We have identified novel antifungal azoles through shape based and pharmacophore based virtual screening. We identified potential CYP51 inhibitors for further investigation, they could also be employed to design ligands with enhanced inhibitory potencies and to predict the potencies of analogs to guide synthesis/or prepare synthetic antifungal analogs against CYP51.

The details are enclosed Annexure-I

12. ACHIEVEMENTS FROM THE PROJECT:

- **The results indicated that both shape-based and pharmacophore-based screening yielded the potential inhibitors.**
- **We have used ligand filtering and virtual screening approaches to identify potential azoles (with imidazoles, 1,2,3 and 1,2,4 triazole scaffolds) from ChemBridge database.**
- **The docking results yielded a potential antifungal compounds with imidazole and triazole scaffolds.**

13. SUMMARY OF THE FINDINGS (IN 500 WORDS):

The incidence of systemic fungal infections has been increased in the last few decades, especially in individuals with immunocompromised hosts, such as patients undergoing anticancer chemotherapy or organ transplants and patients with AIDS. Steol 14α-demethylase (CYP51) is an essential enzyme in the fungal life cycle and also an important target for the antifungal drug development. In the present study, we have implemented a ligand filtering to identify compounds having imidazole, 1,2,3 and 1,2,4 triazole scaffolds, from small molecule ChemBridge database. A three-dimensional model of *Candida albicans* CYP51 (CaCYP51) was constructed and applied to screen against hit compounds filtered through ligand filtering tool. The quality of the model was checked and molecular dynamics simulation was utilized to refine the model. The binding modes of identified azoles were investigated by molecular docking and binding free energy calculation. The identified hit compounds interact with CaCYP51 through π-π stacking, hydrophobic and hydrogen bond interactions. Hydrophobic interactions

were discovered to play significant role in the azoles-CaCYP51 binding. The distance between the nitrogen atom of azoles (N-3 of imidazole and N-4 of triazole) and iron of the heme group varies from 2.23 to 2.32 Å. The searched compounds were also evaluated with ADME properties which show excellent pharmacokinetic properties under the acceptable range. The results indicated that all modeling strategies and screening processes presented in the current study most like to be an encouraging way in search of novel antifungal lead compounds.

14. CONTRIBUTION TO THE SOCIETY (GIVE DETAILS):

***Candida* species are the most common cause of fungal infections. *Candida* species produce infections that range from non—life-threatening mucocutaneous illnesses to invasive processes that may involve virtually any organ. Such a broad range of infections requires an equally broad range of diagnostic and therapeutic strategies. In our study, we have reported the novel antifungal azoles through ligand filtering, shape based and pharmacophore based virtual screening. The reported lead molecules show excellent pharmacokinetic properties**

15. WHETHER ANY PH.D. ENROLLED/PRODUCED OUT OF THE PROJECT:

Ph.D enrolled.

Name of the student: Karnati Konda Reddy

Year of enrollment: 2010

16. NO. OF PUBLICATIONS OUT OF THE PROJECT: **01**

- Karnati Konda Reddy, Sanjeev Kumar Singh, Sunil Kumar Tripathi,Chandrabose Selvaraj, Venkatesan Suryanarayanan. **Shape and pharmacophore-based virtual screening to identify potential cytochrome P450 sterol 14alpha-demethylase inhibitors**. *J Recept Signal Transduct Res* **2013,** *33* (4), 234-43.

Abstracts Published

- Poster in **5th National Symposium cum Workshop on Recent Trends in Structural Bioinformatics and Computer Aided Drug Design (SBCADD-2013)**, 19th-22nd February 2013, held at Alagappa University, Karaikudi, Tamil Nadu. Abstract titled **"Shape and pharmacophore-based virtual screening to identify potential cytochrome P450 sterol 14alpha-demethylase inhibitors".**

- Poster in **Current Trends in Drug Discovery Research (CTDDR-2013)-5th International Symposium on Drug Development for Orphan/Neglected Diseases** 26th-28th February 2013, held at Central Drug Research Institute, Lucknow. Abstract titled **"Discovery of Potential Inhibitors for Cytochrome P450 Sterol 14α-Demethylase from Candida albicans: Shape-based Screening, Homology Modeling and Molecular Docking Study".**

- Poster in **6th National Symposium cum Workshop on Recent Trends in Structural Bioinformatics and Computer Aided Drug Design (SBCADD-2014)**, 18th-21st February 2014, held at Alagappa University, Karaikudi, Tamil Nadu. Abstract titled **"Molecular Modeling and Virtual Screening Approaches for Identification of Candida albicans CYP51 Inhibitors".**

Other Publication

- Karnati Konda Reddy, Sanjeev Kumar Singh, Sunil Kumar Tripathi,Chandrabose Selvaraj. **Identification of potential HIV-1 integrase strand transfer inhibitors: In silico virtual screening and QM/MM docking studies**. *SAR QSAR Environ Res* **2013,** *24* (7), 581-95.

Annexure-I

Introduction

In recent years, life-threatening systemic fungal infections are associated with high morbidity and mortality especially in seriously ill patients (Fridkin and Jarvis, 1996; Wingard and Leather, 2004). The majority of these infections are caused by *Candida* spp., with over 50% due to *Candida albicans* (Richardson and Lass-Florl, 2008; Siwek *et al.*,2012). Several kinds of current clinical antifungal drugs including azoles (such as fluconazole, ketoconazole, and itraconazole), polyenes (such as amphotericin B and nystatin), echinocandins (such as caspofungin and micofungin), and allylamines (such as naftifine and terbinafine) have been developed to reduce the impact of fungal infections (Sheehan *et al.*,1999; Denning, 2002). Among those, azoles have fungistatic, orally active, and broad-spectrum activities against most yeasts and filamentous fungi. They are widely used in antifungal chemotherapy (Sheng *et al.*, 2006). The broad use of azoles has led to development of severe resistance, which significantly reduced the efficacy of them. This situation has led to an ongoing search for new azoles with increased selectivity to combat resistance.

Sterol 14-α demethylase (CYP51) is a member of the cytochrome P450 superfamily, which catalyzes the oxidative removal of the 14α-methyl group of (C-32) lanosterol via three successive monooxygenation reactions to give $\Delta^{14,15}$ –desaturated intermediates in ergosterol biosynthesis. The first two of these reactions are conventional cytochrome P450 hydroxylations that produce the 14-hydroxymethyl and 14-carboxyaldehyde derivatives of lanosterol (Trzaskos *et al.*,1986; Aoyama *et al.*,1987). In the final step, the 14-aldehyde group is eliminated as formic acid with concomitant introduction of $\Delta^{14,15}$ double bond (Fischer *et al.*,1991; Chai *et al.*,2006). CYP51 has been a target for antifungal drug design for decades. Use of standard antifungal therapies is limited for a number of reasons, including toxicity, low efficacy rates, and drug resistance, forcing the development of new antifungal agents with enhanced potency, also the introduction of new classes of antifungal drugs (Podust *et al.*,2004). As an essential enzyme in the fungal life cycle, CYP51 has been a primary target for azole antifungal agents. The azoles have been found as one category of successful broad spectrum CYP51 inhibitors that selectively inhibit this enzyme causing depletion of ergosterol and accumulation of lanosterol and some other 14-methyl sterols and results in growth inhibition of fungal cell (Sangshetti *et al.*,2011). The key interactions in the active site are these components of azoles: (i) the amidine nitrogen atom (N-3 in the

imidazoles, N-4 in the triazoles) to bind the heme iron of enzyme; (ii) aromatic rings; (iii) the large nonpolar portion of molecule (Rezaei *et al.*,2009).

In a continuing effort to find more potent azole antifungal agents, we have used shape-based and pharmacophore-based screening to novel inhibitors. In other study, ligand filtering and virtual screening approaches to identify potential azoles (with imidazoles, 1,2,3 and 1,2,4 triazole scaffolds) from ChemBridge database. On the basis of this strategy, we found new compounds with imidoazole and 1,2,4 triazole scaffolds. Unlike the soluble bacterial P450s, all the fungal CYP51 proteins characterized to date are integral membrane proteins, making structural and biophysical characterization more challenging (Xiao *et al.*,2004). We have constructed three-dimensional (3D) model of *Candida albicans* CYP51 (CaCYP51) through homology modeling on the basis of the crystallographic coordinates of human CYP51. Further, refinement of the generated 3D model was done by subjecting to molecular dynamics (MD) simulations. To get insight into binding mode of identified azole compounds in homology model CaCYP51, we carried out docking studies. The docking results yielded a potential antifungal compounds with imidazole and triazole scaffolds.

Materials and Methods

Antifungal Azoles

We selected the clinically known antifungal azoles classified as imidazoles (Bifonazole, Butoconazole, Clotrimazole, Econazole, Fenticonazole, Isoconazole, Ketoconazole, Miconazole, Omoconazole, Oxiconazole, Sertaconazole, Sulconazole and Tioconazole), triazoles (Albaconazole, Fluconazole, Isavuconazole, Itraconazole, Posaconazole, Ravuconazole, Teroconazole and Voriconazole) and thiazole (abafungin) for common pharmacophore hypothesis (CPH) generation to identify novel and potent inhibitors.

Shape Based Screening

Phase shape is a new shape-based screening method introduced by Schrödinger, which is used to screen the databases against a shape query. Each conformer from a given molecule is aligned to the query in various ways, and a similarity is computed based on overlapping hard-sphere volumes. The conformer and alignment yielding the highest similarity for each molecule is identified based on phase shape similarity (phase sim) score. The shape search treats all atoms as equivalent, or it can incorporate information on atom types. Shape queries investigate a much greater variety of alignments than a typical search for

matches to a hypothesis. A second difference is in the algorithm used to evaluate the volume scores on the one hand, and the shape similarities on the other.

Generation of common pharmacophore hypotheses

The common pharmacophore hypotheses (CPHs) generation for antifungal azoles was carried out by using PHASE. Three-dimensional (3D) conversion and minimization was performed using LigPrep version 2.5 incorporated in PHASE. Conformers were generated using a rapid torsion angle search approach followed by minimization of each generated structure using the OPLS_2005 force field with an implicit GB/SA solvent model. Each minimized conformer was filtered through a relative energy window of 10 kcal mol^{-1} and a minimum atom deviation of 1.0 Å. Each compound structure is represented by a set of points in 3D space, which coincide with various chemical features that may facilitate noncovalent binding between the compound and its target receptor. The pharmacophore features , namely hydrogen bond acceptor (A), hydrogen bond donor (D), hydrophobic group (H), negatively ionizable (N), positively ionizable (P), and aromatic ring (R), were defined by a set of chemical structure patterns using SMARTS queries. Common pharmacophore features were identified from a set of variants–a set of feature types that define a possible pharmacophore using a tree-based partitioning algorithm. The CPHs were scored by setting the root-mean-square deviation (RMSD) value below 1.0, the vector score value to 0.5 and weighing to include consideration of the alignment of inactive compounds using default parameters.

***In silico* virtual screening**

We performed 3D pharmacophore screening using the pharmacophore hypothesis AHHRR representing chemical features of azole inhibitors. Using the hypothesis AHHRR, we search chemical databases and retrieve molecules with novel and desired chemical features from the, Asinex, ChemBridge, and Maybridge databases containing 127,281, 56,391, and 50,000 compounds, respectively. The compounds retrieved from the databases were subjected to *in-silico* screening based on drug-likeness prediction using Lipinski's rule of five, number of rotatable bonds, molecular docking and binding energy. We used semi-flexible docking protocols. The ligands being docked were kept flexible, in order to explore an arbitrary number of torsional degrees of freedom spanned by the translational and rotational parameters. The ligand poses generated were passed through series of hierarchical filters that evaluated the ligands interactions with the receptor. The process of virtual

screening was carried in three phases, using three different docking protocols of docking simulations of varying precisions and computational intensities. High throughput virtual screening (HTVS), Standard precision (SP), extra precision (XP) and Induced Fit Docking protocols were used in this study using the program Glide version 5.7.

Protein preparation

The X-ray crystal structure of Mycobacterium tuberculosis sterol 14α-demthylase MTCYP51 (PDB ID: 1EA1) and homology modeled structure were prepared using Protein Preparation Wizard using default options: bond orders were assigned, hydrogen atoms were added, metals were treated, the gaps in the protein were modeled using prime loop modeling and all crystallographic water molecules were deleted. Hydrogen's were optimized using sample water orientations and the protein was minimized to an RMSD limit from the starting structure of 0.3Å using OPLS_2005 force field.

Ligand Preparation

Clinically used structurally diverse set of antifungal azoles were selected for understanding the binding mode of molecules against MT-CYP51 and CA-CYP51. We also identified the ligands through shape and pharmacophore based screening. These ligands were prepared using the LigPrep module of the Schrödinger suite of tools. First all the hydrogen atoms were added to the ligand molecules as they had implicit hydrogen atoms. The bonds orders of these ligands were fixed. The ionization states of the ligands were generated in the pH range of 5.0-9.0 using epik 2.3. Most probable tautomers and all possible stereo isomers were generated to study the activity of individual stereotypes of each ligand. In the final stage of LigPrep, compounds were minimized with OPLS-2005 Force field.

Molecular Dynamics simulations of MT-CYP51

Molecular Dynamics (MD) Simulations were performed using Desmond, Version 3.1 with OPLS all-atom force field 2005. The X-ray crystal structure of CYP51 from *Mycobacterium tuberculosis* (MT-CYP51) was subjected to 10ns simulations. The water molecules were placed using Desmond, soaking the system with a pre-equilibrated TIP3P model by orthorhombic water box. The distance between box wall and protein was set to be greater than 5 Å, so that the protein did not directly interact with its own periodic image. Minimization of prepared system for MD simulation has been performed upto the maximum

of 3000 steps using the steepest descent until a gradient threshold (25 kcal/mol/ Å) was reached. Further MD simulations were carried on the equilibrated systems for desired period of time at constant temperature of 300K and constant pressure of 1 atm with a time step of 2fs. During the MD simulations smooth Particle-Mesh-Ewald method was used to calculate long range electrostatic interactions. A 9Å cutoff radius value has been used for coulombic short range interaction cutoff method. Frames of trajectory were captured at each 4.8 ps time step. The RMSD of the backbone was calculated through the simulation with the first frame as a reference.

Induced Fit Docking

In standard virtual docking studies, ligands are docked into the binding site of a receptor where the receptor is held rigid and the ligand is free to move. However, the assumption of rigid receptor can give misleading results, since in reality many proteins undergo side-chain or back-bone movements, or both, upon ligand binding. These changes allow the receptor to alter its binding site so that it more closely conforms to the shape and binding mode of the ligand. This is often referred to as "induced fit". The protein structure MTCYP51 (PDB ID.1EA1) was applied with the induced-fit docking (IFD) method in the Schrödinger software suite. IFD methodology uses the docking program Glide to account for ligand flexibility and the Refinement module in the Prime program to account for receptor flexibility. Initial Glide docking of each ligand using a softened potential (van der Waals radii scaling), a maximum 20 poses per ligand are retained, and by default poses to be retained must have a Coulomb-vdW score less than 100 and an H-bond score less than -0.05. The structurally top 20 poses of ligands were used to sample the protein plasticity using the Prime program in the Schrödinger suite. Residues having at least one atom within 5 Å of any of the 20 ligand poses were subjected to a conformational search and minimization process, although residues outside this zone were fixed. In this way, the flexibility of protein was considered. The resulted 20 new receptor conformations were taken forward for redocking. In this redocking stage, Glide docking parameters were set to the default hard-potential function. The Glide XP (extra-precision) was used for all the docking calculations. The binding affinity of each complex was reported in the Glide gscore and also estimated the binding energy (IFD Score) for each output pose.

Phylogenetic Analysis and Homology Modeling

Multiple sequence alignment of CYP51 sequences was performed using the clustalW2 (Larkin et al., 2007). Phylogenetic analysis of CYP51 sequences from *Trypanosoma cruzi* (TC), *Trypanosoma brucei* (TB), *Leishmania infantum* (LI), *Candida albicans* (CA), *Homo sapiens* (HS) and *Mycobacterium tuberculosis* (MC) was performed and evolutionary distances were calculated by maximum composite likelihood method using MEGA (Version.5.05) software (Tamura *et al.*,2011). The sequence of the CaCYP51 was taken from the Uniprot (Accession Code: P10613), and then submitted to BLAST (Basic Local Alignment Search Tool) in search of the homologous protein. Accordingly, the CaCYP51 protein was homology modeled using the crystal structure of human CYP51 (PDB ID: 3LD6) as a structural template. Homology modeling was performed using the Modeller 9v8 software (Eswar *et al.,* 2006). The homology models of CaCYP51 were reported in several papers (Sangshetti *et al.*,2011; Xiao *et al.*,2004). In most of the studies, the membrane spanning domain (residues 1 to 40) was deleted from CaCYP51 prior to modeling. In this study, we modeled complete structure and performed MD simulations of CaCYP51 placing membrane towards N-terminal end (Membrane spanning domain). Further, the CaCYP51 structure was used for molecular docking studies.

Protein Preparation

The homology model structure was prepared by a multi-step process through Protein Preparation Wizard (Schrödinger Suite 2011 Protein Preparation Wizard). The right bond orders as well as charges and atom types were assigned, and hydrogen atoms were added to the structure. The model was subjected to energy minimization using the Optimized Potentials for Liquid Simulations (OPLS)-2005 force field with implicit solvation. The model was minimized and the minimization was terminated when RMSD of heavy atoms in the minimized structure relative to the homology model structure exceeded 0.3 Å.

Molecular Dynamics Simulations

MD Simulations of CaCYP51 was performed using Desmond Molecular Dynamics System (Desmond Molecular Dynamics System, version 3.1, 2012; Guo *et al.,* 2010; Reddy *et al.,* 2014) with the OPLS-AA 2005 force field (Jorgensen et al., 1996; Kaminski *et al.,* 2001). We position the dipalmitoyl phosphatidylcholine (DPPC) lipid bilayer towards the N-terminal region (amino acids 1-40) and equilibrated around 325 K. The protein in the presence of lipid bilayer was immersed in an orthorhombic box containing TIP3P water

molecules and neutralized by adding salt counter-ions. The distance between box wall and system was set to greater than 10 Å to avoid direct interactions with its own periodic image. The energy of prepared systems for MD simulations was minimized up to a maximum of 5000 steps using steepest descent method until a gradient threshold (25 kcal/mol/Å) was reached, followed by LBFGS (Low-memory Broyden-Fletcher-Goldfarb-Shano quasi-Newtonian minimizer) until a convergence threshold of 1 kcal/mol/Å was met. Temperature scale maintained as 300 K for whole simulation using the Nose-Hoover thermostats, and for maintaining stable pressure, Martina-Tobias-Klain barostat method was used. The equations of motion were integrated using the multistep RESPA integrator with an inner time step of 2, 2 and 6 fs for bonded, 'near' nonbonded, and 'far' nonbonded interactions respectively. A 9 Å cutoff was used for the Coulombic interactions, and long-range electrostatics was treated using the particle mesh Ewald method, with a tolerance of $1e^{-9}$ Å. The protein was simulated for 10 ns time period using the parameters described above.

The RMSD, root mean square fluctuation (RMSF) and radius of gyration (RoG) were calculated for the entire simulations trajectory with reference to their respective first frames. An average structure obtained from the MD simulations was used for molecular docking studies.

Ligand preparation and filtering

A total of 50,000 molecules from ChemBridge database were selected for ligand filtering. All the hydrogen atoms were added to the ligand molecules as they only had implicit hydrogen atoms, bond order of these ligands were fixed and ionization states of ligands were generated in the pH range of 5.0-9.0 using Epik during ligand preparation by LigPrep (LigPrep, version 2.5, 2012). Most probable tautomers and all possible stereo isomers were generated to study the activity of individual stereotypes of each ligand. In the final stage of LigPrep, compounds were minimized with OPLS-2005 force field. After running the ligand preparation a total of 91,169 ligands were generated. The compounds having imidazole, 1,2,3 and 1,2,4 triazole scaffolds (Fig.1) were identified from ChemBridge database using the Ligand filtering tool (Ligand Filter, 2012).

Structure-based virtual screening

The compounds identified through Ligand filtering tool were docked into the binding site of the CaCYP51. Potential binding pocket was identified using the default parameters in

the program of SiteMap (SiteMap, version 2.6, 2012) from Schrödinger. We ran high throughput virtual screening (HTVS), standard precision (SP) and extra precision (XP) protocols using the program Glide (Glide, version 5.8, 2012; Friesner *et al.,* 2006). In docking simulation, we used semi-flexible docking protocols. The ligands being docked were kept flexible, in order to explore an arbitrary number of torsional degrees of freedom spanned by the translational and rotational parameters. The ligand poses generated were passed through series of hierarchial filters that evaluated ligand interaction with its receptor.

Prime MM-GBSA binding free energy

The top docked poses for each ligand were rescored for calculation of binding free energy by Prime/MMGBSA method (Prime, version 3.1, 2012). The docked poses were minimized using the local optimization feature in Prime, and the energies of complex were calculated using the OPLS-AA 2005 force field and generalized-Born/surface area (GB/SA) continuum solvent model. The binding free energy (ΔG_{bind}) was calculated using the following equation (Lyne *et al.,* 2006):

$$\Delta G_{bind} = \Delta_E + \Delta G_{solv} + \Delta G_{SA} \quad (1)$$

$$\Delta E = E_{complex} - E_{protein} - E_{ligand} \quad (2)$$

where $E_{complex}$, $E_{protein}$, and E_{ligand} are the minimized energies of the protein-ligand complex, protein, and ligand, respectively

$$\Delta G_{solv} = G_{solv(complex)} - G_{solv(protein)} - G_{solv(ligand)} \quad (3)$$

where $G_{solv(complex)}$, $G_{solv(protein)}$, and $G_{solv(ligand)}$ are the solvation free energies of the complex, protein, and ligand, respectively

$$\Delta G_{SA} = G_{SA(complex)} - G_{SA(protein)} - G_{SA(ligand)} \quad (4)$$

where $G_{SA(complex)}$, $G_{SA(protein)}$, and $G_{SA(ligand)}$ are the surface area energies for the complex, protein and ligand, respectively (Tripathi *et al.,* 2013).

ADME Studies

The ligands identified in this study were subjected to predict the pharmacokinetic properties using QikProp (QikProp, version 3.5, 2012). Accurate prediction of absorption, distribution, metabolism, excretion (ADME) properties prior to experimental procedures can eliminate unnecessary testing of compounds. The percentage of their human oral absorption was also predicted to determine their toxicity levels.

Results and Discussion

Shape based screening

Shape-based screening has proven to be a valuable tool in computer-aided drug design, especially in the context of virtual screening. Additionally, they have other successful applications, such as scaffold hopping, bioisostere replacement, virtual library design, and flexible ligand superposition. Shape-based screening with electrostatic treatment of the atoms is an attractive method because highly similar molecules in this context should have highly similar binding characteristics. Indeed, shape-based methods have proven to perform well in virtual screening calculations when compared with other methods. The phase_shape program is used to screen the database against a shape query generated for the fluconazole bound to MT-CYP51 shown in Fig.1. Each conformer from a given molecule is aligned to the query in various ways, and a similarity is computed based on overlapping hard-sphere volumes. The conformer and alignment yielding the highest similarity for each molecule are identified. We used an atom type (pharmacophore) to use in volume scoring. The volume overlaps used to compute the similarity are only calculated for atoms of the same type. Shape queries investigate a much greater variety of alignments than a typical search for matches to a hypothesis.

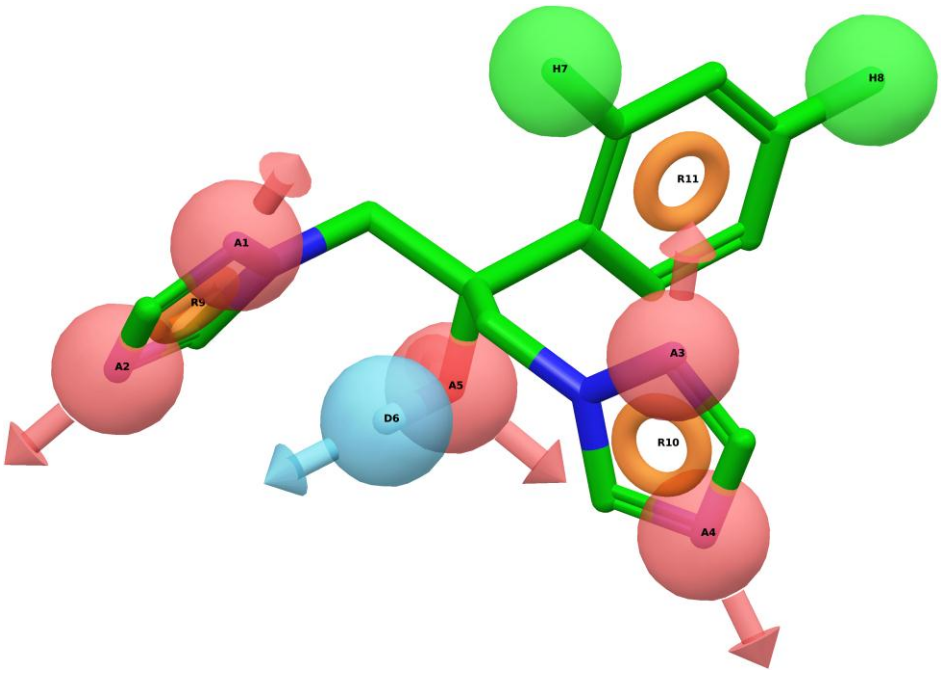

Figure 1: Conformation of fluconazole with pharmacophore bound to MTCYP51. It is used for shape based screening to find novel inhibitors.

Pharmacophore based screening

The best common pharmacophore hypothesis AHHRR with distances is shown in Fig.2. The angles of pharmacophore hypothesis AHHRR are given in Table 1. Based on the CPH AHHRR three chemical databases, namely, Asinex, ChemBridge and Maybridge containing diverse chemical compounds were screened using PHASE. The compounds retrieved from the database were subjected to various screening based on Fitness score, drug-likeness prediction using Lipinski's rule of five and number of rotatable bonds that should be <=7.

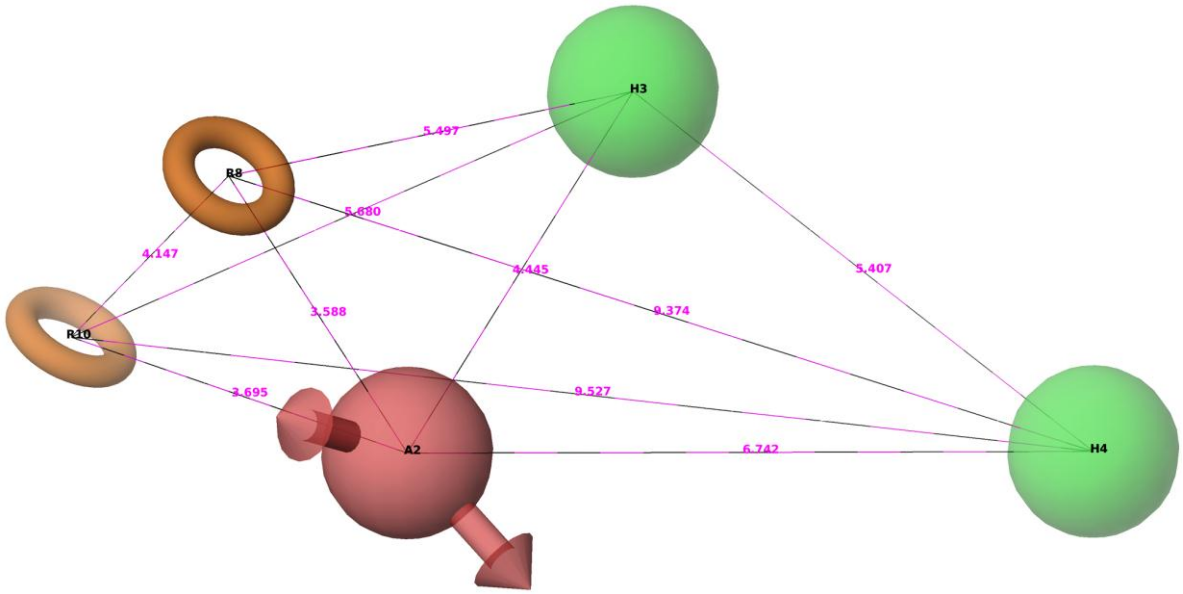

Figure 2: Common Pharmacophore Hypothesis (CPH) AHHRR; intersite distances in Å between pharmacophore features. Spheres with vectors A2 (red) is acceptor feature, spheres H3 and H4 (green) are hydrophobic, and R8 and R10 (orange) are aromatic features.

Table 1: Angles of pharmacophore hypothesis AHHRR.

Site1	Site2	Site3	Angle (degree)[a]
H3	A2	H4	53.1
H3	A2	R8	85.7
H3	A2	R10	88
H4	A2	R8	127.6
H4	A2	R10	129.4
R8	A2	R10	69.4
A2	H3	H4	85.8
A2	H3	R8	40.6

A2	H3	R10	40.5
H4	H3	R8	118.6
H4	H3	R10	118.5
R8	H3	R10	43.5
A2	H4	H3	41.1
A2	H4	R8	17.6
A2	H4	R10	17.4
H3	H4	R8	31
H3	H4	R10	31.6
R8	H4	R10	25.3
A2	R8	H3	53.7
A2	R8	H4	34.7
A2	R8	R10	56.5
H3	R8	H4	30.4
H3	R8	R10	70.6
H4	R8	R10	79.4
A2	R10	H3	51.4
A2	R10	H4	33.1
A2	R10	R8	54.1
H3	R10	H4	29.9
H3	R10	R8	65.9
H4	R10	R8	75.3

[a]Angle degree of site1-site2-site3

In silico virtual screening

The process of molecular docking was carried on the filtered compounds using virtual screening workflow of Schrödinger using three different protocols of docking simulations of varying precisions and computational intensities. All the virtual hits were docked using the high-throughput virtual screening (HTVS) protocol, which is least computationally intense process intended for rapid screening of the ligands. Approximately 10% ligands were selected for standard precision docking based on docking score. Further, we identified 10 compounds using extra precision molecular docking and binding energy analysis. The flowchart of screening is shown in Fig.3. Based on the results of molecular docking to the active site of CYP51, we identified some novel inhibitors which show good docking score and interaction with active site amino acids. Analysis of the binding mode of reported antifungal azoles and identified compounds at the active site of the MT-CYP51 revealed the interaction with the conserved active site residues.

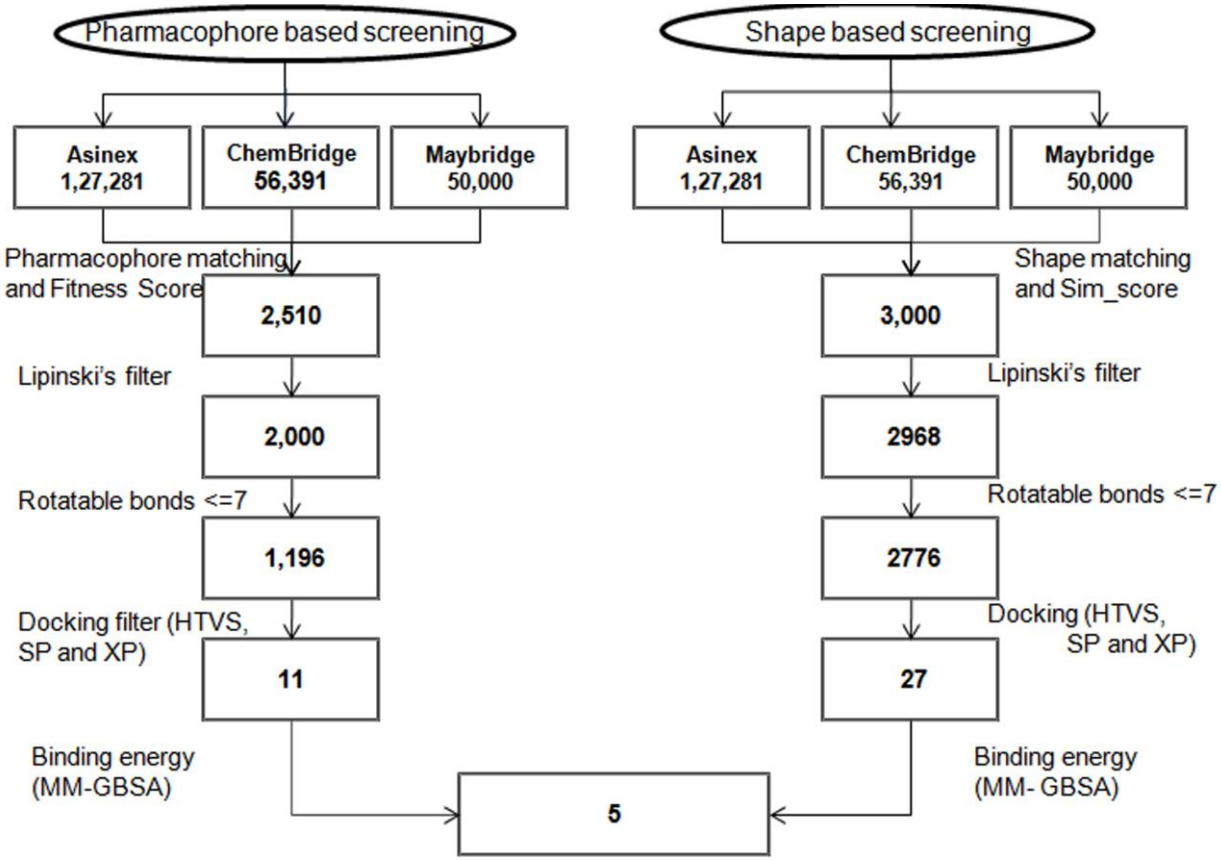

Figure 3: Flowchart for *in silico* virtual screening using both pharmacophore and shape based screening.

Molecular Dynamics simulations of MT-CYP51

We performed MD simulation of 10ns on X-ray crystal structure of MT-CYP51 to check the stability; RMSD graph of MT-CYP51 is shown in Fig.4, as per the graph, structure got stabilized at the later part of the simulation after deviating around 2Å with reference to the first. MT-CYP51 showed a very little standard deviation (0.19) during the 10ns simulation, which shows its high structural compactness and stability.

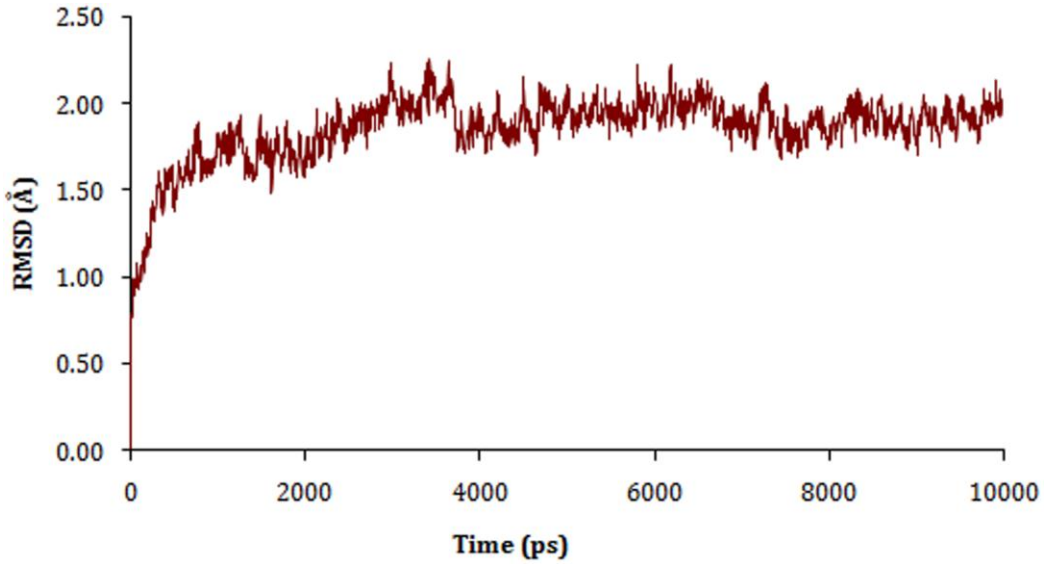

Figure 4: RMSD of the backbone for the MT-CYP51 X-ray crystal structure as a function of the simulation time.

Induce Fit Docking

With the aim of investigating dynamic behavior of the active site during the binding of ligand, we performed IFD on antifungal azoles (imidazoles, triazoles and thiazole) using the X-ray crystal structure MT-CYP51. The crystal structure used for the study is fluconazole-bound MT-CYP51, this is the first structure of an authentic p450 drug target. The IFD ligand interactions of imidazoles are shown in Fig.5, triazoles in Fig.6 and thiazole (abafungin) in Fig.7. The IFD results are listed in Table 2.

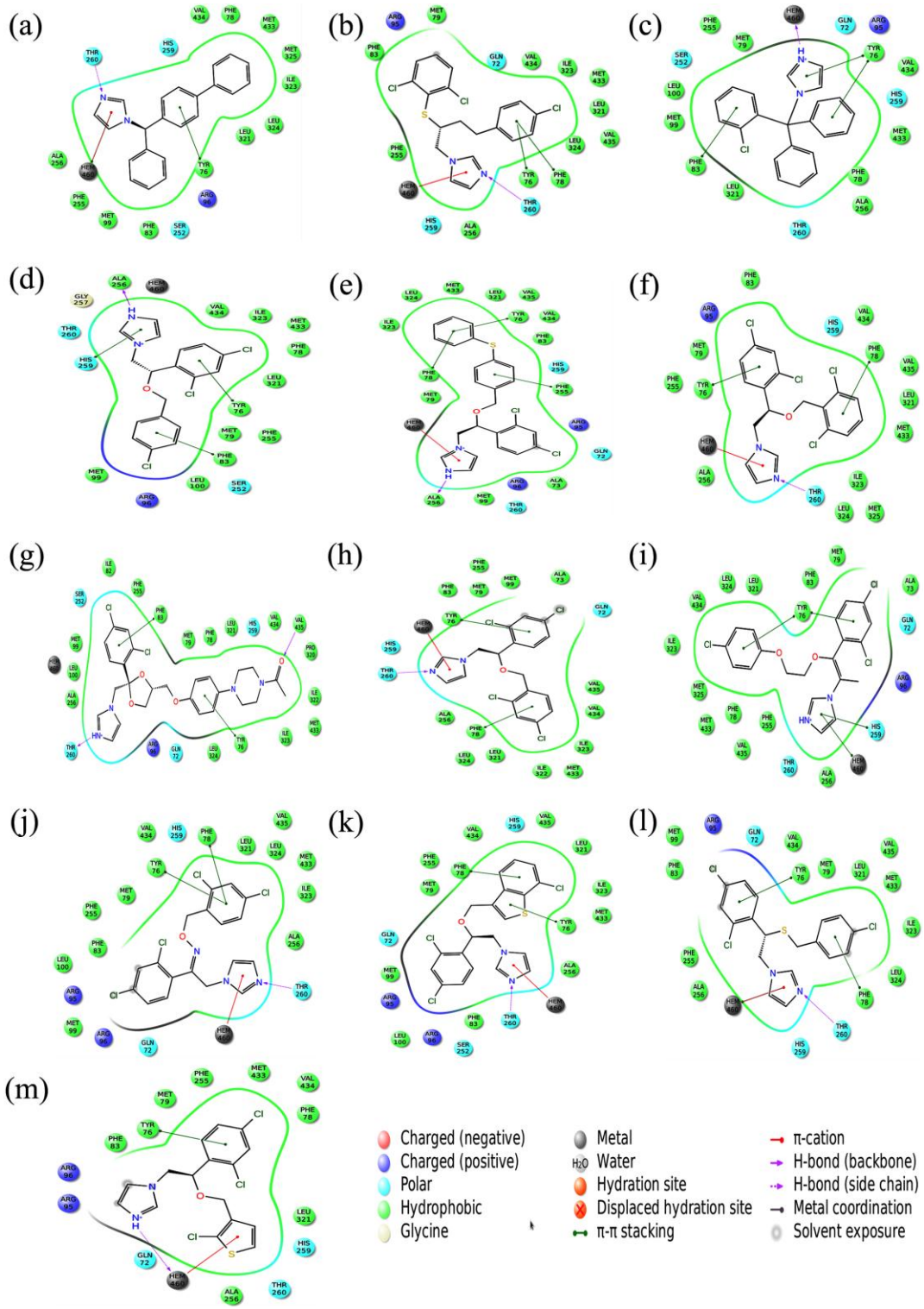

Figure 5: Structures of the imidazoles bound to the MTCYP5.(a) Bifonazole (b) Butoconazole (c) Clotrimazole (d) Econazole (e) Fenticonazole (f) Isoconazole (g) Ketoconazole (h) Miconazole (i) Omoconazole (j) Oxiconazole (k) Sertaconazole (l) Sulconazole (m)Tioconazole .

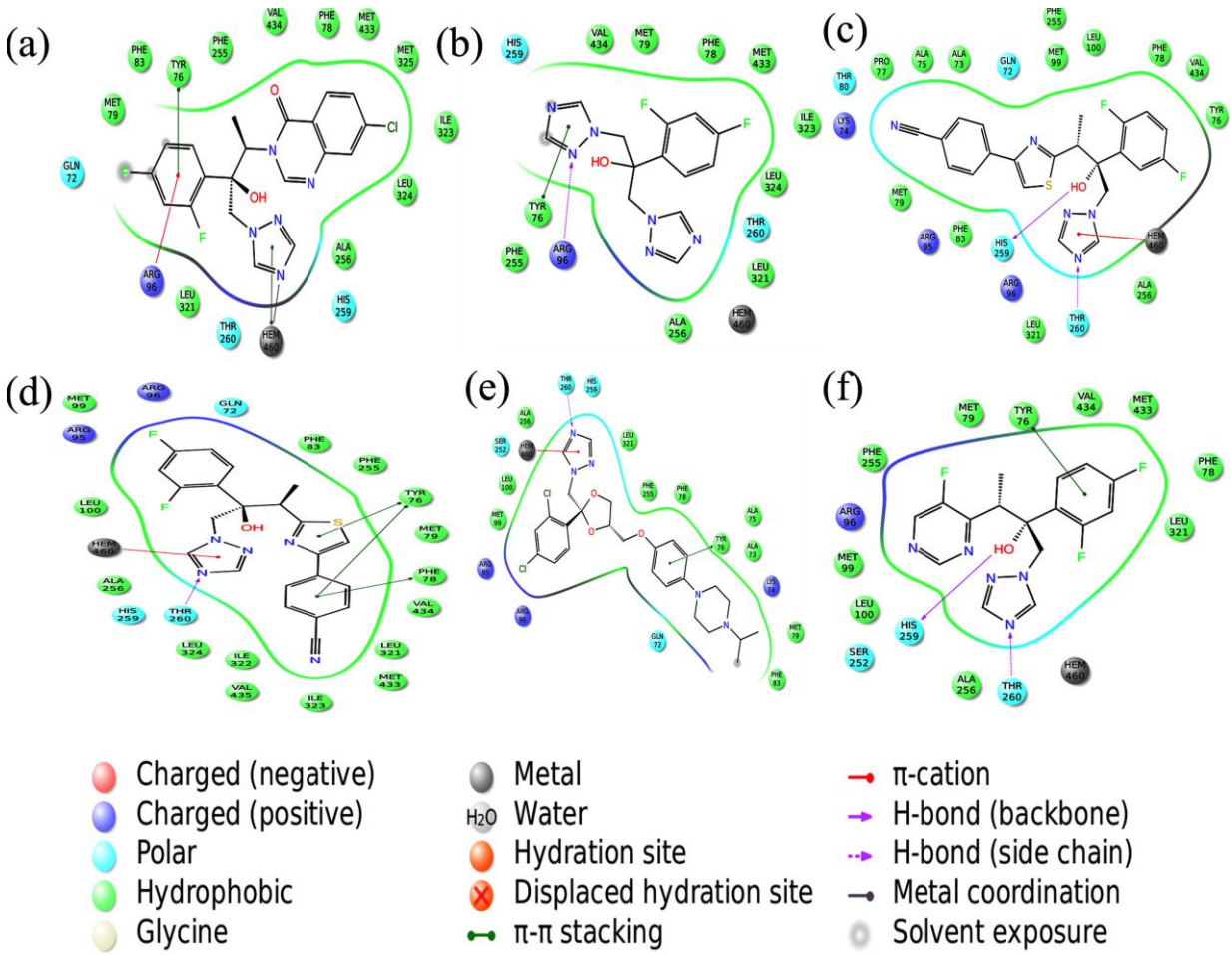

Figure 6: Structures of the triazoles bound to the MTCYP5. (a) Albaconazole (b) Fluconazole (c) Isavuconazole (d) Ravuconazole (e) Teroconazole (f) Voriconzole.

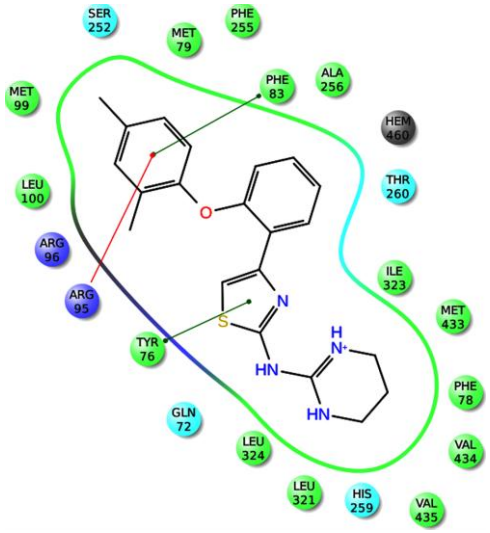

Figure 7: Structure of the thiazole (Abafungin) bound to the MTCYP51

Table 2: Induced-Fit Docking Results of antifungal azoles.

S.No	Compound Name	XP GScore	IFD Score	Emodel Score
1	Bifonazole	-10.45	-1018.82	-73.44
2	Butoconazole	-11.54	-1021.94	-95.7
3	Clotrimazole	-9.96	-1017.15	-57.57
4	Econazole	-10.66	-1021.99	-94.09
5	Fenticonazole	-12.17	-1025.36	-102.79
6	Isoconazole	-10.78	-1019.57	-84.32
7	Oxiconazole	-11.35	-1020.36	-90.59
8	Sertaconazole	-11.32	-1022.5	-90.4
9	Sulconazole	-9.74	-1019.52	-79.65
10	Tioconazole	-10.34	-1019.86	-83.57
11	Omoconazole	-9.62	-1020.65	-94.79
12	Miconazole	-10.13	-1021.45	-96.81
13	Ketoconazole	-11.75	-1023.90	-125.14
14	Abafungin	-8.617	-1022.19	-87.25
15	Albaconazole	-7.96	-1016.74	-74.21
16	Fluconazole	-6.874	-1012.73	-69.41
17	Isavuconazole	-10.8	-1021.09	-127.45
18	Ravuconazole	-10.76	-1021.27	-106.42
19	Voriconazole	-8.49	-1017.58	-69.9

Sequence Alignment and Phylogenetic Analysis

The multiple sequence alignment of the protein sequences of CA-CYP51, *Homo sapiens* (HS)-CYP51, *Trypanosoma brucei* (TB)-CYP51, *Trypanosoma cruzi* (TC)-CYP51,

Leishmania infantum (LI)-CYP51, MT-CYP51 is shown in Fig.8. The phylogram shown in Fig.9 tells that CA-CYP51 and HS-CYP51 are orthologous.

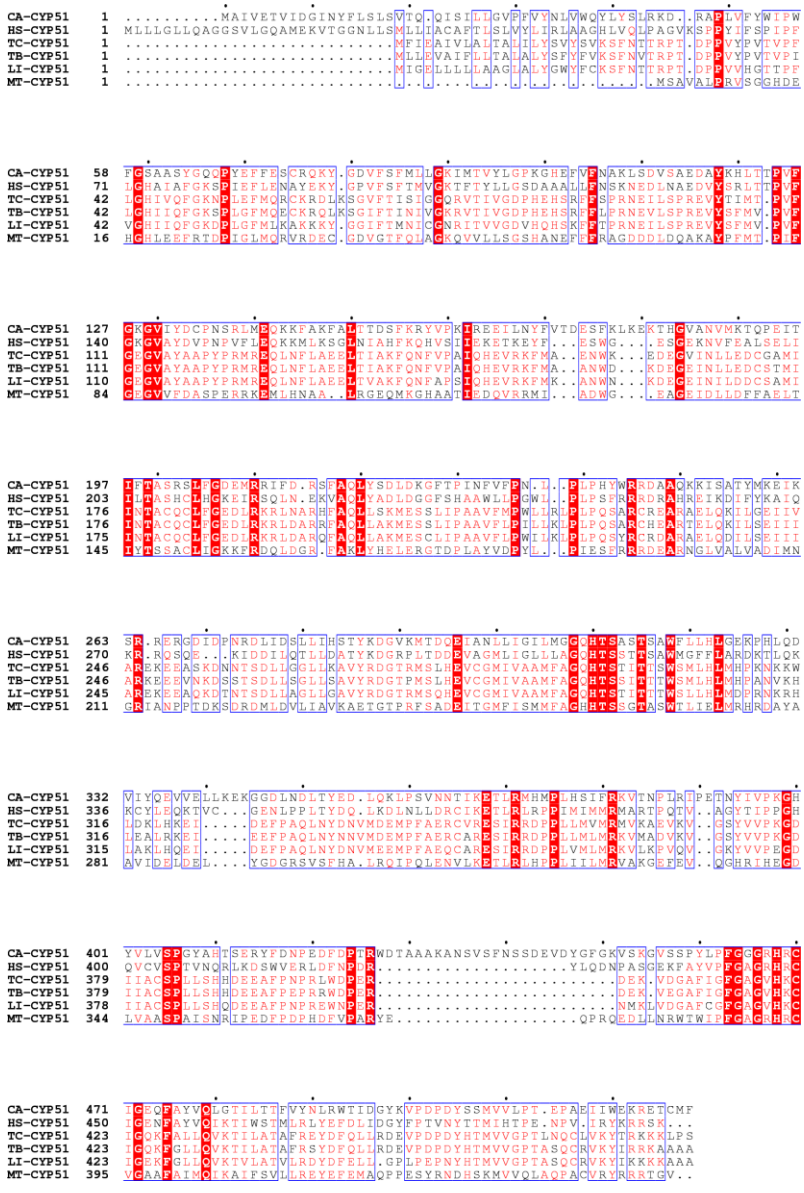

Figure 8: Alignment of the amino acid sequences of human CYP51 with CA-CYP51, TC-CYP51, TB-CYP51, L-CYP51 and MB-CYP51. Conserved regions among different CYP51 were highlighted with red color.

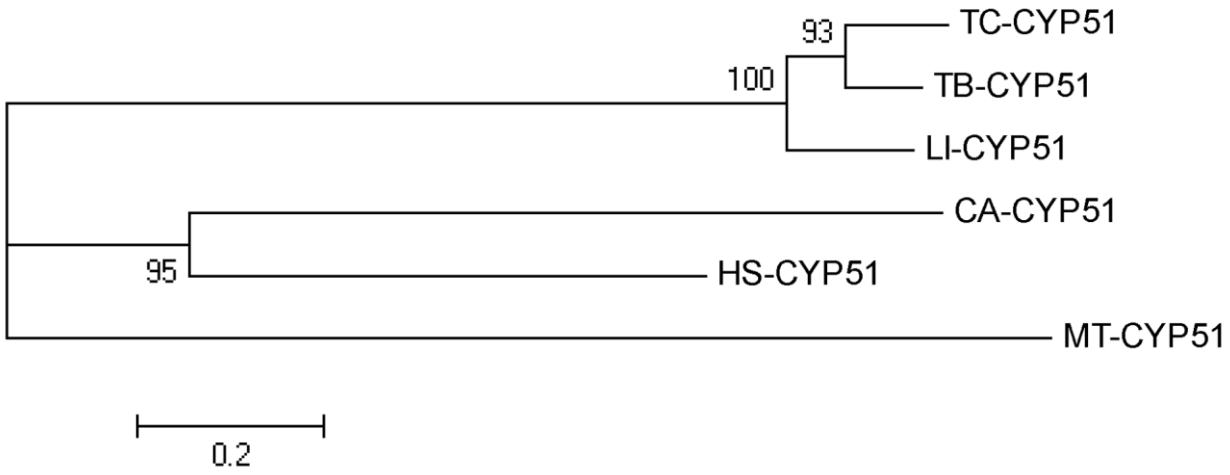

Figure 9: The phylogram tree is generated using the program Mega. In the above figure the branch lengths of the 6 sequences are proportional to the amount of inferred evolutionary change. CA-CYP51 and HS-CYP51 are orthologous.

Homology modeling

We have constructed the homology model of CA-CYP51 from human CYP51 enzyme shown in Fig.10. The Ramachandran plot of psi and phi backbone conformational angles for each residue in the protein can be seen in Fig.11. The data from the Ramachandran plot reveals that 89.1% of the amino acid residues are in the most favorable regions and 9.5% of the amino acids are in additional allowed regions, 0.5% in generously allowed and 1% in disallowed regions. The overall good model quality (Z-score=-8.74) when analyzed by the ProSA software.

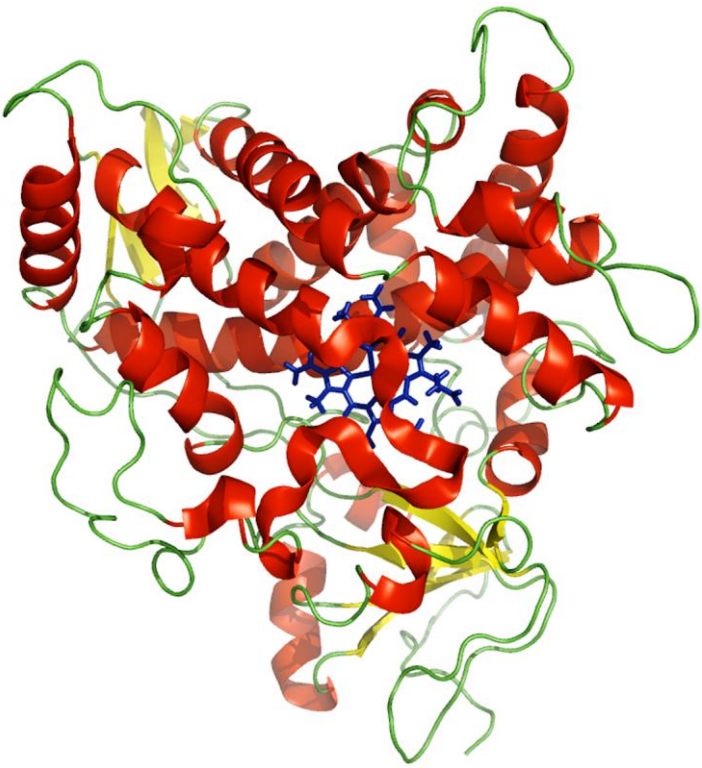

Figure 10: Homology model structure of *Candida albicans* CYP51. Helices and strands are shown in red and yellow. Heme factor is highlighted in blue.

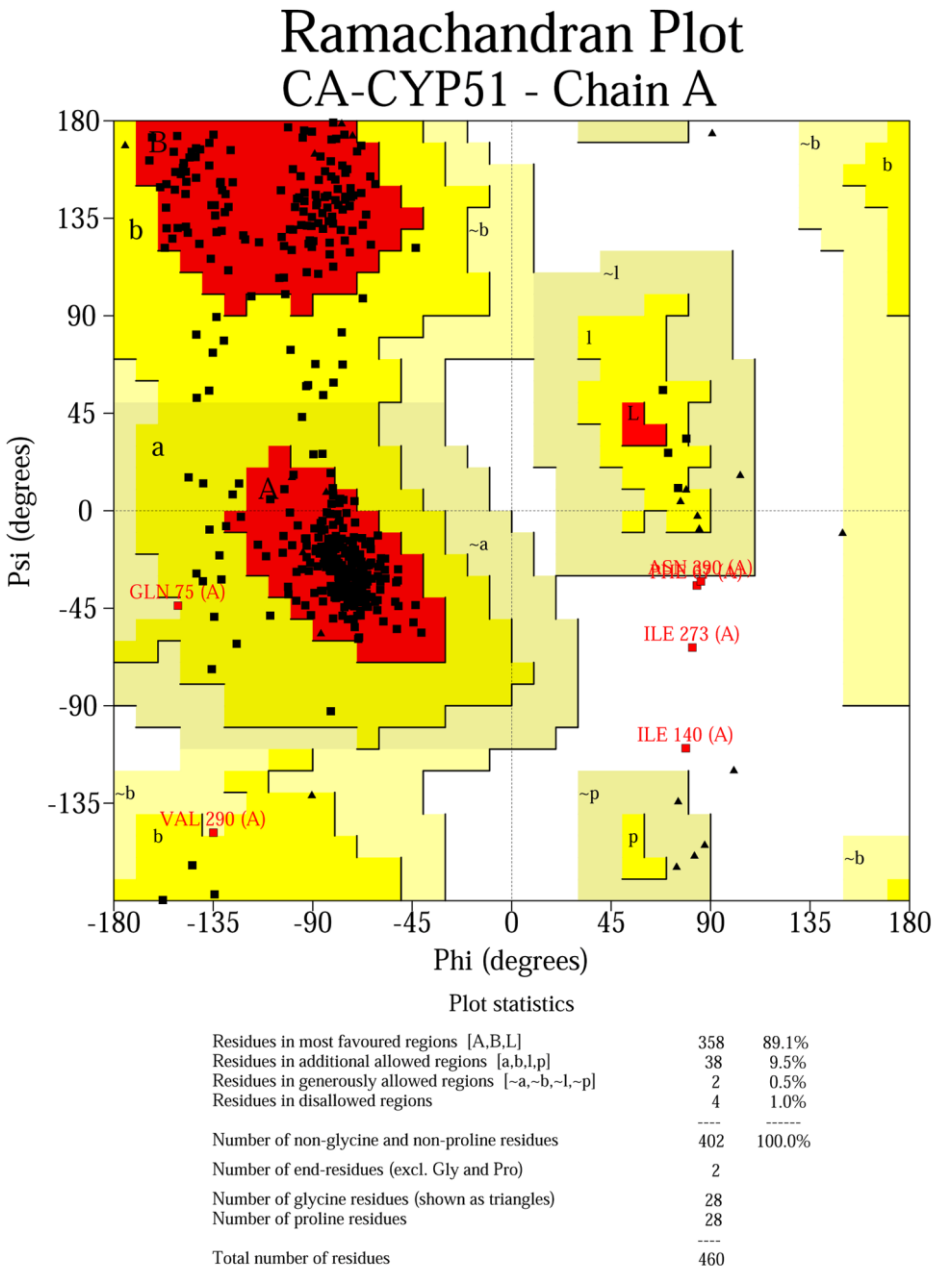

Figure 11: Ramachandran plot of homology modeled structure of CA-CYP51.

Molecular Dynamics Simulations

MD simulation of CaCYP51 was performed by placing membrane towards N-terminal region (Fig. 12). MD simulation of the CaCYP51 was carried out in order to evaluate the stability of the homology model. Analysis of dynamics shows that the CaCYP51 is stable after 4000 ps (Fig. 13). The CaCYP51 does not show major structure conformational changes in comparison to the initial model, which is consistent with the relatively low RMSD

values. The overall atomic fluctuation of CaCYP51 during the 10 ns time scale of the MD simulation was also calculated and is shown in Fig. 14. These results indicate that the protein has many flexible motifs. The loop containing residues 420-430 fluctuate from 1 Å to 6.5 Å. The active site of CaCYP51 is a deep, hydrophobic cavity in the centre of the enzyme contains the heme cofactor. RoG is a measure of the compactness of the protein structure. Less the deviation in the RoG means more the compactness of the structure is conserved. Rog of the CaCYP51 was stable throughout the 10 ns MD simulation (Fig. 15).

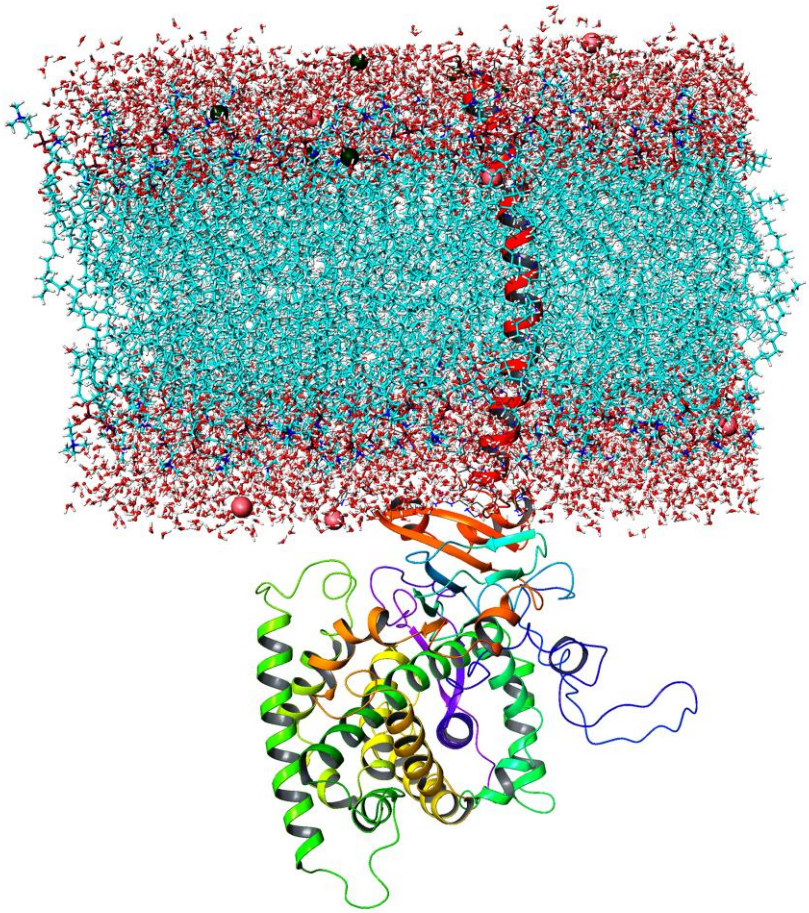

Figure 12: Homology model structure of *Candida albicans* CYP51. DPPC lipid bilayer is placed towards the membrane spanning domain *i.e.,* N-terminal region (1-40 amino acids).

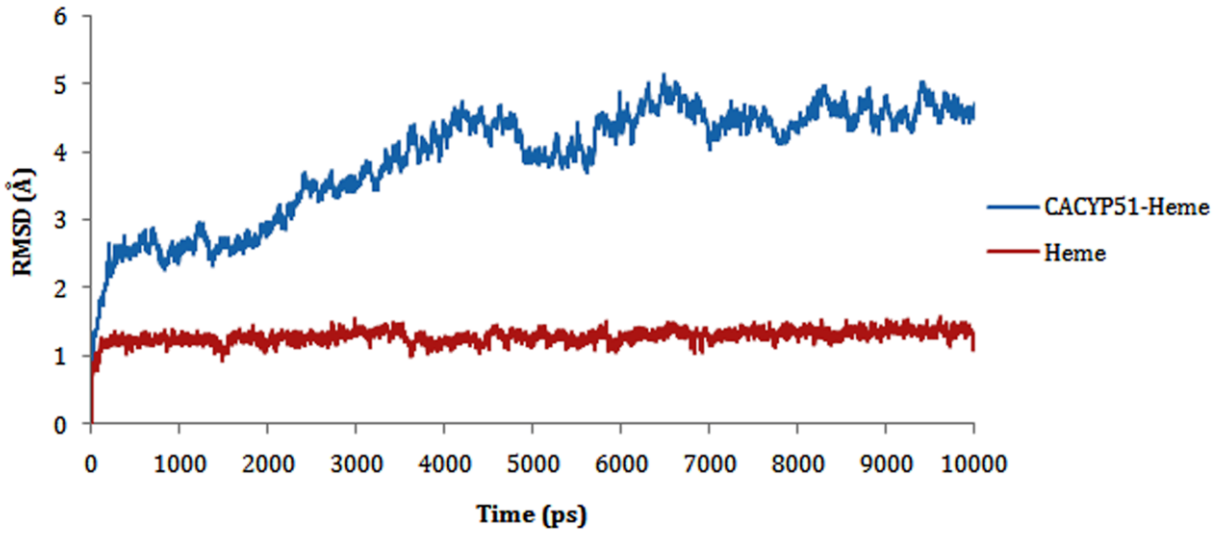

Figure 13: RMSD plot for the backbone of CaCYP51-Heme complex and heavy atoms of Heme during the MD simulations.

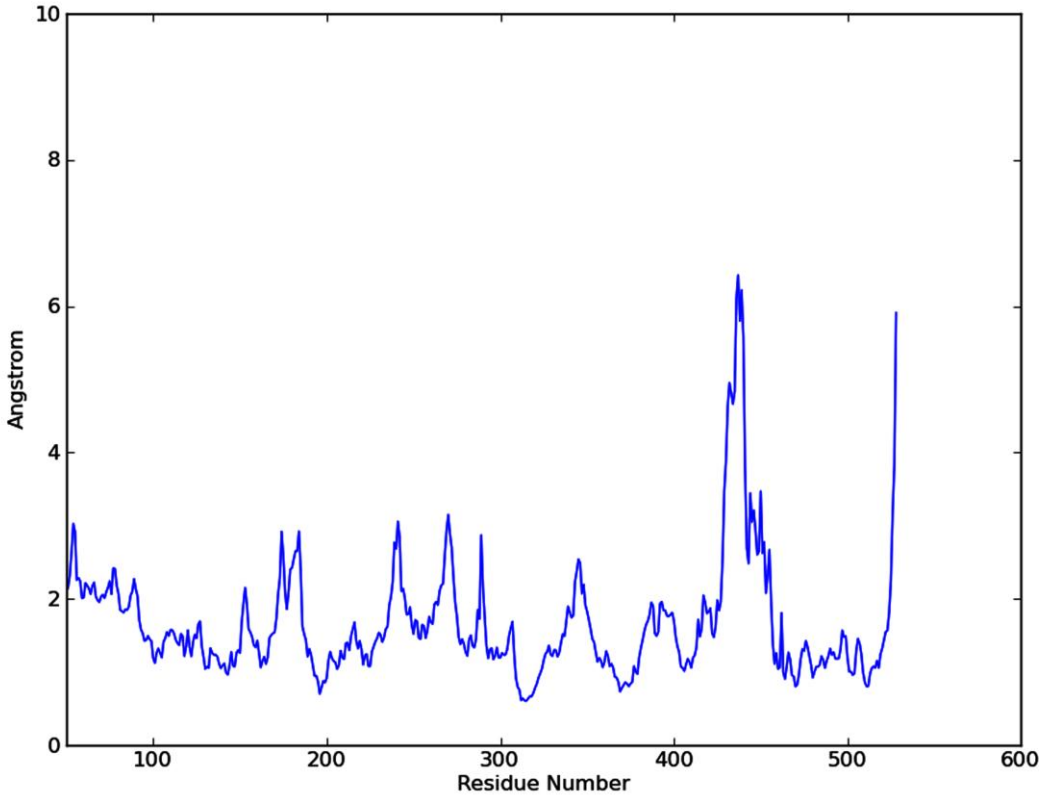

Figure 14: RMSF of CaCYP51 through function of time.

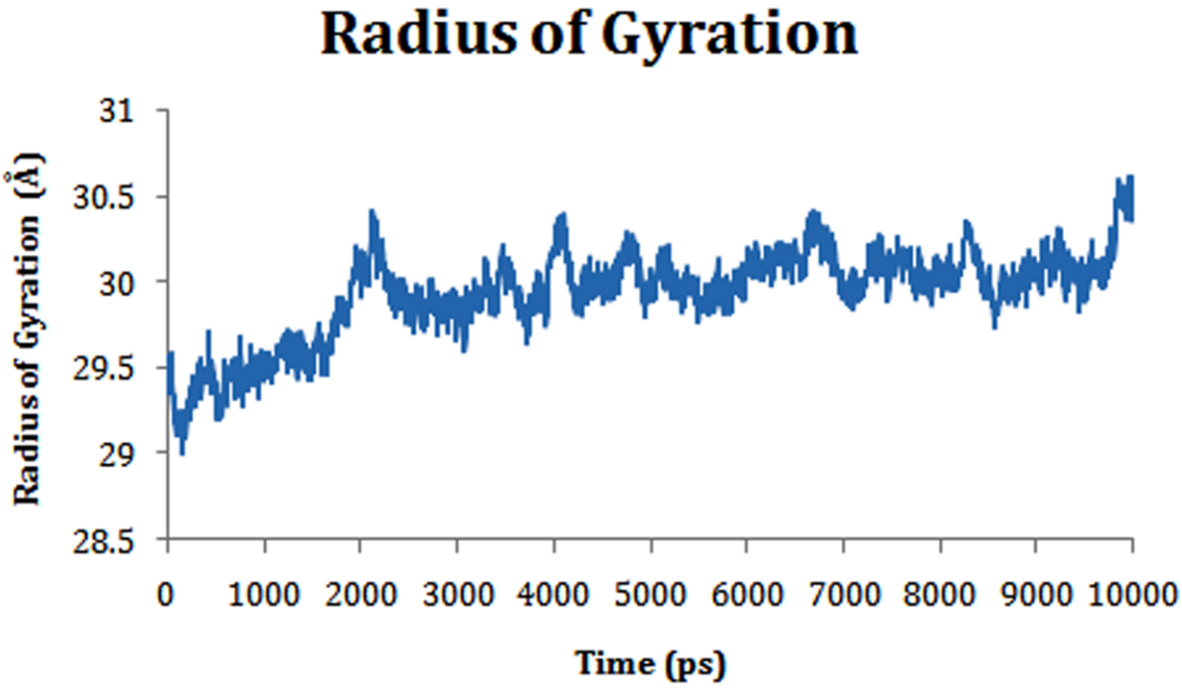

Figure 15: The backbone of radius of gyration (R_g) plotted as the function of simulation time.

Ligand preparation and filtering

ChemBridge database was searched for imidazole and triazole scaffolds (**Fig. 16**). Azoles with a substituent different from a hydrogen in the α positions were excluded. Compounds containing imidazole, 1,2,3 and 1,2,4 triazole scaffolds, were extracted from the database through ligand filtering. We identified 2,449 compounds having imidazole, 1,2,3 and 1,2,4 triazole scaffolds. This choice is based on the knowledge that aromatic heterocycles are able to inhibit P450 enzymes by coordinating the iron atom in heme, thus preventing oxygen binding and subsequent oxidation reaction of the substrate.

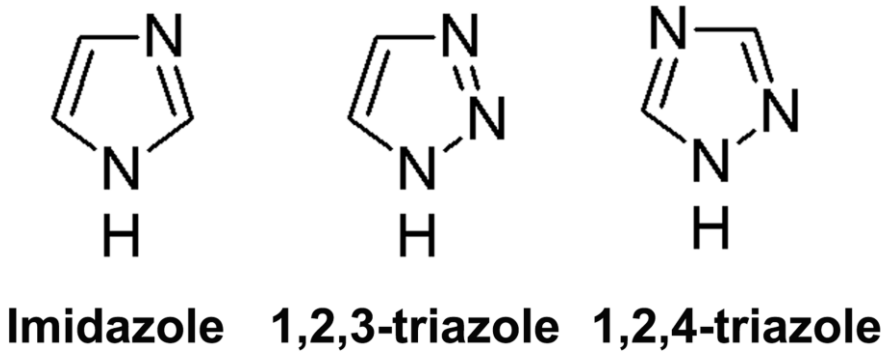

Figure16: ChemBridge database is filtered for compounds having Imidazole, 1,2,3 and 1,2,4 triazole scaffolds through Ligfilter.

Structure-based virtual screening

The selected azoles filtered through ligand filtering tool were docked into the binding pocket of CaCYP51 by focusing on the satisfaction of metal binding.. A three-tiered docking screen was then performed. In the first screen a filtered selection of the ChemBridge database containing about 2,449 compounds were docked into the active site of CaCYP51, using the HTVS protocol, which is least computationally intense process intended for rapid screening of the ligands. The top 10% ligands were selected for SP docking based on docking score. Finally, we identified total of six compounds using XP docking and visual inspection.

Binding mode and free energy analysis

The binding modes are analyzed for the best six compounds identified through ligand filtering and structure-based virtual screening (Fig. 17). We found in all the best hit compounds nitrogen atom N-3 of an imidazole ring and nitrogen atom N-4 of 1,2,4 triazole ring coordinates the iron of the heme group. Out of six compounds, three compounds having 1,2,4 triazole scaffold and three having imidazole scaffold. The docking score, hydrophobic contacts and the distance between nitrogen atom (N-3 in imidazole and N-4 in triazole) of azoles and the iron of the heme group are shown in Table 3. The distance between nitrogen atom of the azole heterocyclic ring and heme iron is less than 2.32 Å. ChemBridge_ID 41638749 interacts with Met306 and Pro375 via hydrogen bond interactions. The heterocyclic ring of ChemBridge_ID 29855504 exhibits hydrogen bond interaction with Met508, and π-cation interaction with His310. From the above mentioned interaction residues His310 is proven to be in S1 pocket that represents the hydrophilic site, which is defined by Gln309, His310 and Ser312. The NH group of ChemBridge_ID 98398298 and hydroxyl group of ChemBridge_ID 16730187 forms hydrogen bond interaction with Ser378. The amino acid Ser378 is a well validated residue for the hydrogen-bonding interactions (Wang *et al.,* 2009). Aside, π-π interaction formed between azole and heme. ChemBridge_ID 28061079 form hydrogen bond interaction with Met508. In addition, the compound makes π-stacking interactions with Phe228 and heme. ChemBridge_ID 24315513 also forms hydrogen bond interaction with Met508, and π- stacking interaction with Tyr118 and heme. All the six compounds bind to the S2 pocket through the formation of a coordination bond with the iron

atom of the heme group. The S2 pocket is above the heme ring representing the core hydrophobic area. The docking outcomes for six compounds show a common binding mode with the iron of the heme group (Fig. 18). Few compounds formed π-stacking interaction with Try118. The amino acid Tyr118 is a highly conserved residue through the CYP51 family, and site-directed mutagenesis of corresponding Tyr76 of MtCYP51 has revealed its importance in maintaining proper orientation of the heme. Therefore, Tyr118 may be an important residue for the CaCYP51 inhibitors. All the six compounds show hydrophobic contacts with Tyr118, Phe228, Leu376 and Met508. The hydrophobic interactions are most commonly seen in identified hits. Hydrophobic contacts are shown with considerable number of residues of the hydrophobic active site. Hydrophobic interactions play a pivotal role in compound binding and these residues contribute to substrate specificity of CYP51 from various species. Analysis of the binding site interactions of identified compounds at the active site of the CaCYP51 revealed the interactions with the conserved active site residues, which are significantly conserved through evolution in plants, mammals and fungi.

Table 3: Docking results for the azole compounds docked in CaCYP51.

S.No	ChemBridge_ID	XP GScore[a]	Hydrophobic interactions	Distance (Å)[b]
1	41638749	-8.09	Tyr118, Phe228, Leu375, Met508 and Val509	2.29
2	29855504	-8.17	Tyr118, Tyr132, Phe228, Leu376, Met508 and Val509	2.32
3	98398298	-8.22	Tyr118, Phe228, Met306, Leu376, Met508 and Val509	2.28
4	16730187	-7.65	Tyr118, Tyr132, Phe228,	2.23

			Leu376 and Met508	
5	28061079	-8.22	Phe126, Ile131, Phe228, Leu376 and Val509	2.32
6	24315513	-7.55	Tyr118, Tyr132, Phe228, Leu376 and Met508	2.28

[a]XP GScore is the predicted binding energy using Glide in kcal/mol

[b]Distance between nitrogen atom of azole compounds and iron atom of heme group

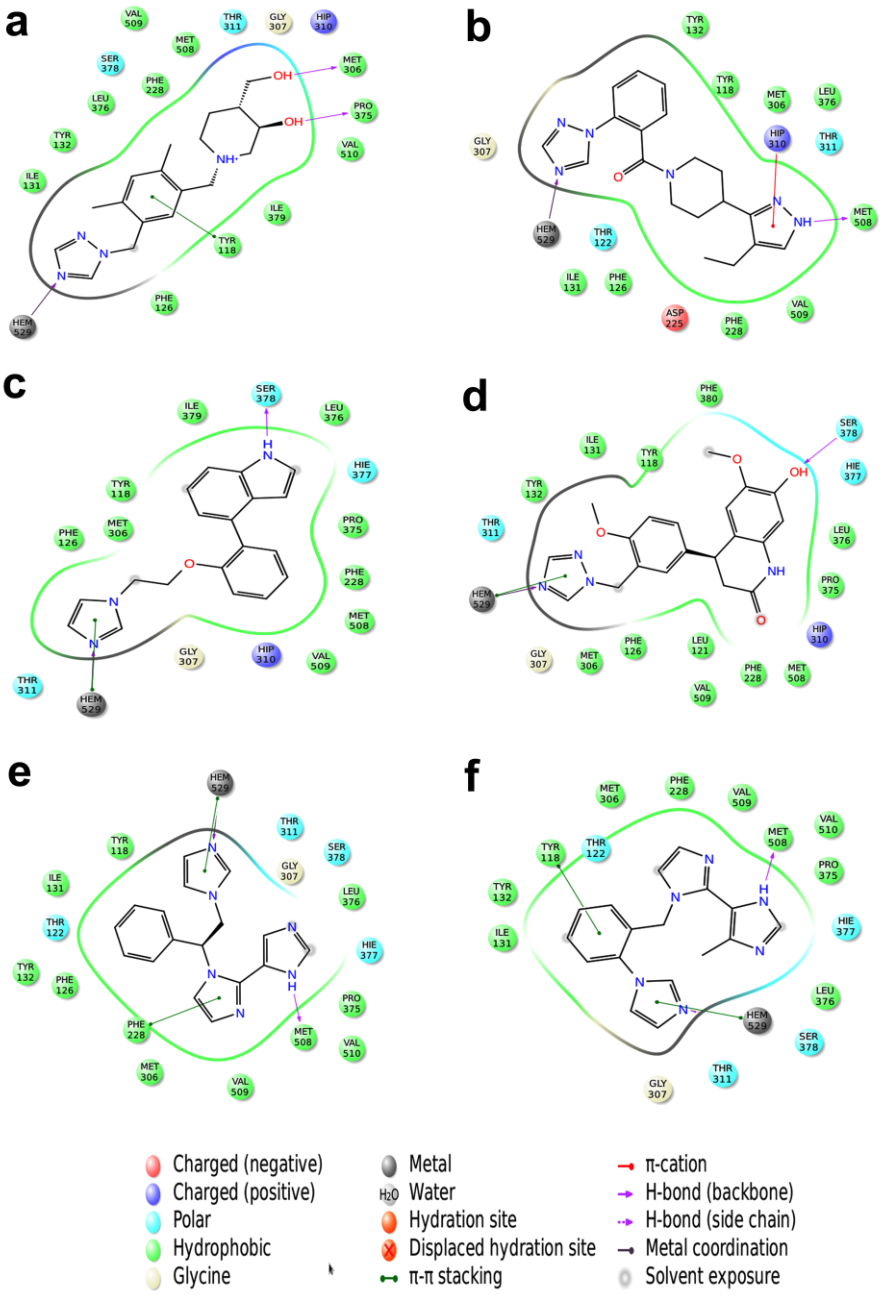

Figure 17: Ligand interaction diagrams of best six azole compounds identified through Ligand filtering and structure-based virtual screening. (a) ChemBridge_ID 41638749. (b) ChemBridge_ID 29855504. (c) ChemBridge_ID 98398298. (d) ChemBridge_ID 16730187. (e) ChemBridge_ID 28061079. (f) ChemBridge_ID 24315513.

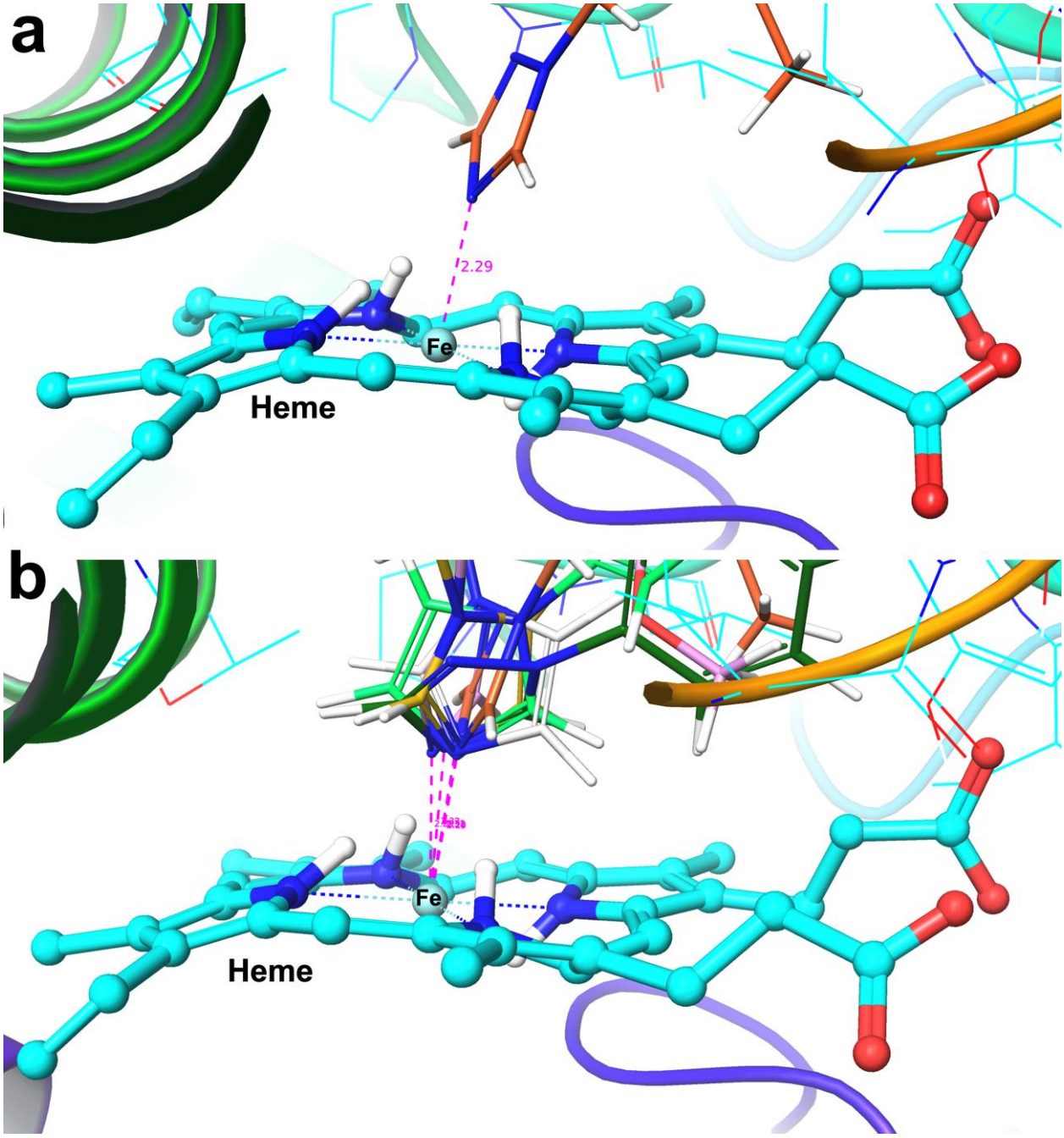

Fig. 18 The distance between nitrogen atom of azole and iron atom in heme group. (a) The distance between nitrogen atom (N-4) of azole and iron atom in heme. (b) The six compounds are superimposed and distances are shown between nitrogen atom (N-3 in imidazole and N-4 in triazole) and iron atom in heme

The calculated binding free energies (ΔG_{bind}) of the CaCYP51 with identified azoles range from -46.79 to -68.75 kcal/mol. According to the energy components of the binding

free energies (Table 4), the major favorable contributors to ligand binding are van der Waals, electrostatic interactions and non-polar solvation terms (ΔG_{SA}). The polar solvation (ΔG_{solv}) opposes binding. The predicted pharmacological properties of the identified compounds were in the ranges predicted by QikProp for 95% of know oral drugs (Table 5). The identified azole compounds could be promising leads for the discovery of novel antifungal agents.

Table 4 Binding free energy calculation results for azoles bound with CaCYP51. All energies are in kcal/mol

S.No	ChemBridge_ID	$\Delta G_{Coulomb}$[a]	ΔG_{vdW}[b]	$\Delta G_{Covalent}$[c]	ΔG_{solv}[d]	ΔG_{SA}[e]	ΔG_{bind}[f]
1	41638749	-23.59	-40.68	7.47	47.23	-41.37	-52.19
2	29855504	-44.13	-43.35	1.99	68.31	-42.11	-60.41
3	98398298	-56	-33.44	-0.75	64	-34.13	-61.44
4	16730187	-46.01	-42.79	3.98	62.2	-33.83	-57.76
5	28061079	-53.81	-33.36	5.47	64.01	-26.7	-46.79
6	24315513	-80.06	-34.81	5.08	68.12	-24.98	-68.75

[a] Coulomb energy
[b] van der Waals energy
[c] covalent energy (internal energy)
[d] Generalized born electrostatic solvation energy
[e] surface area due to lipophilic energy (nonpolar contribution estimated by solvent accessible surface area)
[f]Free energy of binding

Table 5 Predicted properties of azole compounds from QikProp

S.No	ChemBridge_ID	QPlogPo/w [a]	QPlogS [b]	QPPCaco2 [c]	Percent Human Oral Absorption [d]

1	41638749	1.358	-1.66	193.564	75.827
2	29855504	2.48	-4.294	526.762	90.178
3	98398298	4.726	-5.254	2553.303	100
4	16730187	2.421	-4.416	356.315	86.795
5	28061079	3.022	-3.935	862.224	100
6	24315513	2.961	-4.097	963.701	100

[a]Log of the octanol/water partition coefficient (acceptable range: -2 to 6.5)
[b]Log of aqueous solubility S (mol/L) (acceptable range: -6.5 to 0.5)
[c]Caco2 cell permeability in nm/s (acceptable range: <25 is poor and >500 is great)
[d]Percentage of Human Oral Absorption (<25% is poor and >80% is great)

Conclusion

Selective inhibition of CYP51 would cause depletion of ergosterol and accumulation of lanosterol and 14-methyl sterols resulting in the growth inhibition of fungal cells. In this study, We used Shape-based and pharmacophore-based virtual screening for the identification of novel inhibitors. Further, ligand filtering and virtual screening were successfully used to identify new azoles with imidazole and triazole scaffold. The structural information of CaCYP51 was used to screen to novel antifungal agents. In summary, we identified six compounds with imidazole and 1,2,4 triazole scaffolds binds to the active site through the formation of a coordination bond with the iron atom of the heme group. All the six compounds interacted with active site of CaCYP51 mainly through hydrophobic contacts with Tyr118, Phe228, Leu376 and Met508. The identified compounds could be promising leads, they may show better selectivity toward CaCYP51 than marketed azole antifungal agents.

References

Aoyama, Y., Yoshida, Y., Sonoda, Y., Sato, Y. 1987. Metabolism of 32-hydroxy-24,25-dihydrolanosterol by purified cytochrome P-45014DM from yeast. Evidence for

contribution of the cytochrome to whole process of lanosterol 14 alpha-demethylation. The Journal of Biological Chemistry 262, 1239-1243.

Chai, X., Zhang, J., Hu, H., Yu, S., Sun, Q., Dan, Z., Jiang, Y., Wu, Q. 2009. Design, synthesis, and biological evaluation of novel triazole derivatives as inhibitors of cytochrome P450 14alpha-demethylase. European Journal of Medicinal Chemistry 44, 1913-1920.

Denning, D.W. 2002. Echinocandins: a new class of antifungal. Journal of Antimicrobial Chemotherapy 49, 889-891.

Desmond Molecular Dynamics System, version 3.1, D. E. Shaw Research, New York, NY, 2012. Maestro-Desmond Interoperability Tools, version 3.1, Schrödinger, New York, NY, 2012.

Eswar, N., Webb, B., Marti-Renom, M.A., Madhusudhan, M.S., Eramian, D., Shen, M.Y., Pieper, U., Sali, A. 2006. Comparative protein structure modeling using Modeller. Current protocols in bioinformatics / editoral board, Andreas D Baxevanis [et al] Chapter 5, Unit 5 6.

Fischer, R.T., Trzaskos, J.M., Magolda, R.L., Ko, S.S., Brosz, C.S., Larsen, B. 1991. Lanosterol 14 alpha-methyl demethylase. Isolation and characterization of the third metabolically generated oxidative demethylation intermediate. The Journal of Biological Chemistry 266, 6124-6132.

Fridkin, S.K., Jarvis, W.R. 1996. Epidemiology of nosocomial fungal infections. Clinical Microbiology Reviews 9, 499-511.

Friesner, R.A., Murphy, R.B., Repasky, M.P., Frye, L.L., Greenwood, J.R., Halgren, T.A., Sanschagrin, P.C., Mainz, D.T. 2006. Extra precision glide: docking and scoring incorporating a model of hydrophobic enclosure for protein-ligand complexes. Journal of Medicinal Chemistry 49, 6177-6196.

Glide, version 5.8, Schrödinger, LLC, New York, NY, 2012.

Guo, Z., Mohanty, U., Noehre, J., Sawyer, T.K., Sherman, W., Krilov, G. 2010. Probing the alpha-helical structural stability of stapled p53 peptides: molecular dynamics simulations and analysis. Chemical Biology & Drug Design 75, 348-359.

Jorgensen, W.L., Maxwell, D.S., Tirado-Rives, J. 1996. Development and Testing of the OPLS All-Atom Force Field on Conformational Energetics and Properties of Organic Liquids. Journal of the American Chemical Society 118, 11225-11236.

Kaminski, G.A., Friesner, R.A., Tirado-Rives, J., Jorgensen, W.L. 2001. Evaluation and Reparametrization of the OPLS-AA Force Field for Proteins via Comparison with Accurate Quantum Chemical Calculations on Peptidases. The Journal of Physical Chemistry B 105, 6474-6487.

Larkin, M.A., Blackshields, G., Brown, N.P., Chenna, R., McGettigan, P.A., McWilliam, H., Valentin, F., Wallace, I.M., Wilm, A., Lopez, R., Thompson, J.D., Gibson, T.J., Higgins, D.G. 2007. Clustal W and Clustal X version 2.0. Bioinformatics 23, 2947-2948.

Ligand Filter, Schrödinger, LLC, New York, NY, 2012.

LigPrep, version 2.5, Schrödinger, LLC, New York, NY, 2012.

Lyne, P.D., Lamb, M.L., Saeh, J.C. 2006. Accurate prediction of the relative potencies of members of a series of kinase inhibitors using molecular docking and MM-GBSA scoring. Journal of Medicinal Chemistry 49, 4805-4808.

Podust, L.M., Yermalitskaya, L.V., Lepesheva, G.I., Podust, V.N., Dalmasso, E.A., Waterman, M.R. 2004. Estriol bound and ligand-free structures of sterol 14alpha-demethylase. Structure 12, 1937-1945.

Prime, version 3.1, Schrödinger, LLC, New York, NY, 2012.

QikProp, version 3.5, Schrödinger, LLC, New York, NY, 2012.

Reddy, K.K., Singh, P., Singh, S.K. 2014. Blocking the interaction between HIV-1 integrase and human LEDGF/p75: mutational studies, virtual screening and molecular dynamics simulations. Molecular Biosystems 10, 526-536.

Rezaei, Z., Khabnadideh, S., Pakshir, K., Hossaini, Z., Amiri, F., Assadpour, E. 2009. Design, synthesis, and antifungal activity of triazole and benzotriazole derivatives. European of Journal of Medicinal Chemistry 44, 3064-3067.

Richardson, M., Lass-Florl, C. 2008. Changing epidemiology of systemic fungal infections. Clinical Microbiology and Infection 14 Suppl 4, 5-24.

Sangshetti, J.N., Lokwani, D.K., Sarkate, A.P., Shinde, D.B. 2011. Synthesis, antifungal activity, and docking study of some new 1,2,4-triazole analogs. Chemical Biology & Drug Design 78, 800-809.

Schrödinger Suite 2011 Protein Preparation Wizard; Epik version 2.3, Schrödinger, LLC, New York, NY, 2012; Impact version 5.8, Schrödinger, LLC, New York, NY, 2012; Prime version 3.1, Schrödinger, LLC, New York, NY, 2012.

Sheehan, D.J., Hitchcock, C.A., Sibley, C.M. 1999. Current and emerging azole antifungal agents. Clinical Microbiology Reviews 12, 40-79.

Sheng, C., Zhang, W., Ji, H., Zhang, M., Song, Y., Xu, H., Zhu, J., Miao, Z., Jiang, Q., Yao, J., Zhou, Y., Zhu, J., Lu, J. 2006. Structure-based optimization of azole antifungal agents by CoMFA, CoMSIA, and molecular docking. Journal of Medicinal Chemistry 49, 2512-2525.

SiteMap, version 2.6, Schrödinger, LLC, New York, NY, 2012.

Siwek, A., Stefanska, J., Dzitko, K., Ruszczak, A. 2012. Antifungal effect of 4-arylthiosemicarbazides against Candida species. Search for molecular basis of antifungal activity of thiosemicarbazide derivatives. Journal of Molecular Modeling 18, 4159-4170.

Tamura, K., Peterson, D., Peterson, N., Stecher, G., Nei, M., Kumar, S. 2011. MEGA5: molecular evolutionary genetics analysis using maximum likelihood, evolutionary distance, and maximum parsimony methods. Molecular Biology and Evolution 28, 2731-2739.

Tripathi, S.K., Muttineni, R., Singh, S.K. 2013. Extra precision docking, free energy calculation and molecular dynamics simulation studies of CDK2 inhibitors. Journal of Theoretical Biology 334, 87-100.

Trzaskos, J.M., Fischer, R.T., Favata, M.F. 1986. Mechanistic studies of lanosterol C-32 demethylation. Conditions which promote oxysterol intermediate accumulation during the demethylation process. The Journal of Biological Chemistry 261, 16937-16942.

Wang, W., Sheng, C., Che, X., Ji, H., Cao, Y., Miao, Z., Yao, J., Zhang, W. 2009. Discovery of highly potent novel antifungal azoles by structure-based rational design. Bioorganic & Medicinal Chemistry Letters 19, 5965-5969.

Wingard, J.R., Leather, H. 2004. A new era of antifungal therapy. Biology of Blood and Marrow Transplantation 10, 73-90.

Xiao, L., Madison, V., Chau, A.S., Loebenberg, D., Palermo, R.E., McNicholas, P.M. 2004. Three-dimensional models of wild-type and mutated forms of cytochrome P450 14alpha-sterol demethylases from Aspergillus fumigatus and Candida albicans provide insights into posaconazole binding. Antimicrobial Agents and Chemotherapy 48, 568-574.